Journal of Power Sources 228 (2013) 244–249

Contents lists available at SciVerse ScienceDirect

Journal of Power Sources

journal homepage: www.elsevier.com/locate/jpowsour

Ru-doped $Li_4Ti_5O_{12}$ anode materials for high rate lithium-ion batteries

Wei Wang [a], Hualing Wang [b], Shubo Wang [a], Yuejiao Hu [a], Qixiang Tian [b], Shuqiang Jiao [a,*]

[a] School of Metallurgical and Ecological Engineering, University of Science and Technology Beijing, Beijing, 100083, PR China
[b] The First Scientific Research Institute of Wuxi, Wuxi 214035, PR China

HIGHLIGHTS

- Synthesis of Ru doped lithium titanate by a reverse microemulsion method.
- Ru doped lithium titanates had an excellent electrochemical performance.
- Ru doped lithium titanates remained high capacity under a large cycled rate.

ARTICLE INFO

Article history:
Received 7 August 2012
Received in revised form
7 October 2012
Accepted 24 November 2012
Available online 30 November 2012

Keywords:
Lithium-ion batteries
Lithium titanate
Ruthenium
Anode materials

ABSTRACT

Ruthenium doped nanostructured lithium titanates have been synthesized through a reverse microemulsion method with a subsequent sintering process. The as-prepared powders are characterized by the X-ray diffraction and transmission electron microscope techniques. The results indicate that a solid solution of $Li_4Ti_{5-x}Ru_xO_{12}$ is formed when x was less than 0.1. The electrochemical performances of the as-prepared materials are investigated in a potential range from 0.01 to 2.5 V by charge and discharge characterizations. In that, the as-prepared $Li_4Ti_{4.95}Ru_{0.05}O_{12}$ exhibits an excellent electrochemical performance. The specific discharge capacity remains as 131 mAh g^{-1} over 100 cycles even cycled at a large density of 17,500 mA g^{-1} (60 C-rate). While the current density decreases to be 875 mA g^{-1}(3 C-rate), the corresponding specific discharge capacity is kept as high as 259 mAh g^{-1} after 100 cycles.

1. Introduction

Lithium ion batteries are currently used as power sources for many portable electronic devices, power tools and electrical vehicles, such as mobile phones, notebook computers and hybrid electric vehicles due to their high energy density and long cycle life [1–3]. Spinel $Li_4Ti_5O_{12}$ is a promising material for lithium ion batteries [4–7]. Compared to the currently used graphite, this material exhibits characteristic properties [8], such as very flat voltage plateau at around 1.55 V *vs.* Li/Li^+ and very small structural change during charge and discharge processes, so it is also called zero-strain insertion material [9–11].

However, $Li_4Ti_5O_{12}$ suffers from a problem of poor rate capability mainly due to its low electric conductivity (10^{-9} S cm^{-1}) [12]. Substituting Li or Ti by other metals is the main method to modify $Li_4Ti_5O_{12}$ in order to improve electric conductivity. So far, some of metallic elements such as Mg, V, Mn, Fe, Cr, Ta, Ni, Al, Sn and so on are investigated to modify $Li_4Ti_5O_{12}$ [13–19].

Charge and discharge measurements of $Li_4Ti_5O_{12}$ were usually performed in a potential range of 0.5–2.5 V *vs.* Li. Recently, the potential range of 0–2.5 V have been reported to enhance the total specific capacity of $Li_4Ti_5O_{12}$ [14,15,20–22].

In this work, nano-sized spinel $Li_4Ti_5O_{12}$ doped by Ru was synthesized in a reverse microemulsion through sintering the precursor to form a solid solution. As the content of Ru-doping was optimized, the product showed excellent electrochemical properties for energy storage in the charge–discharge range of 0–2.5 V.

2. Experimental methods

All materials and chemicals were purchased commercially and used as received. The Li–Ti–Ru–O precursors were synthesized by a reverse microemulsion method. The reverse microemulsion was prepared as follows: 60 mL n-hexane, 60 mL n-hexanol and 30 mL TritonX-100 were mixed together as the oil phase in a conical flask, followed by the addition of 8 mL of 1 mol L^{-1} $LiOH\cdot H_2O$ and 8 mL water solution of $RuCl_3$ as the water phase, and the mole ratio of Li:Ru is 4:x (x = 0, 0.05, 0.10, 0.15).

After stirred for 1 h, tetrabutyl titanate [$Ti(OC_4H_9)_4$] was gradually dropped into the solution under stirring. The starting materials,

* Corresponding author. Tel./fax: +86 10 62334204.
E-mail address: sjiao@ustb.edu.cn (S. Jiao).

0378-7753/$ – see front matter © 2012 Elsevier B.V. All rights reserved.
http://dx.doi.org/10.1016/j.jpowsour.2012.11.092

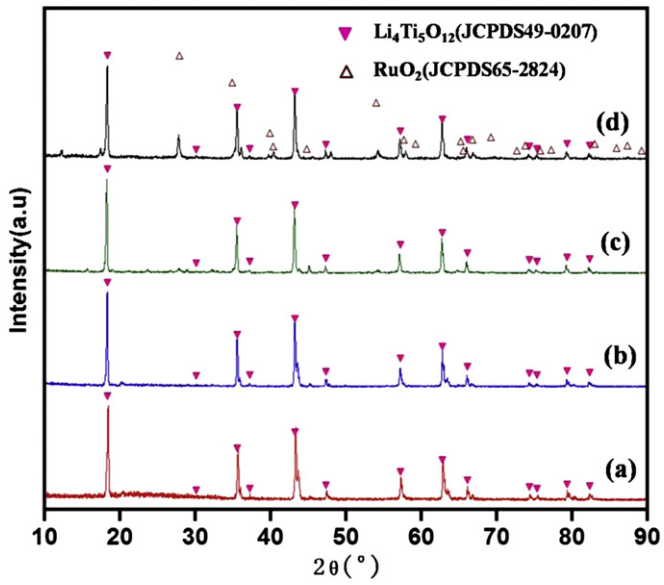

Fig. 1. XRD patterns of the four samples calcined at 850 °C (a) $Li_4Ti_5O_{12}$ (b) Li:Ru = 4:0.05 (c) Li:Ru = 4:0.10 (d) Li:Ru = 4:0.15.

LiOH and tetrabutyl titanate, were mixed in a Li:Ti molar ratio of 4:5 − *x*. After stirred for 5 h, the organic matter was removed with alcohol by a centrifuge. The above mixture was dried in an oven at 60 °C for 12 h and then heated in a muffle furnace for 4 h at 850 °C. The four samples were labeled as sample 1 to sample 4, correspondingly the mole ratio of Li:Ru was 4:*x* (*x* = 0, 0.05, 0.10, 0.15).

The structure and morphology of the as-prepared materials were characterized by X-ray diffraction measurement (XRD, Rigaku, D/max-RB) and transmission electron microscopy (TEM, JEOL, JEM-2010).

The working electrode was fabricated by mixing the active material $Li_4Ti_5O_{12}$ doped by Ru, MWCNTs (multiwalled carbon nanotubes) and teflon (poly(tetrafluoroethylene), PTFE) binder in a weight ratio of 75:15:10. The compounds above were put into an ultrasonic vibration generator to mix uniformly. The mixtures were dried at 60 °C in an oven until they became slurries and then pasted uniformly onto a copper foil and dried at 120 °C for above 12 h. Tablet machine was used to make the electrode smooth and thin and after that, the electrode was cut into rounded pieces with a diameter of about 8 mm. The electrochemical characterizations were measured by means of the coin-type cell CR2032. The active material electrode was used as the working electrode, and Li foil was used for both counter and reference electrodes with 1.0 M $LiPF_6$ in an electrolyte solution (EC/DMC/EMC = 1/1/1, V/V/V); the cell was then assembled as a coin cell. The cell assembly was carried out in a glove box filled with high-purity argon gas. Charge and

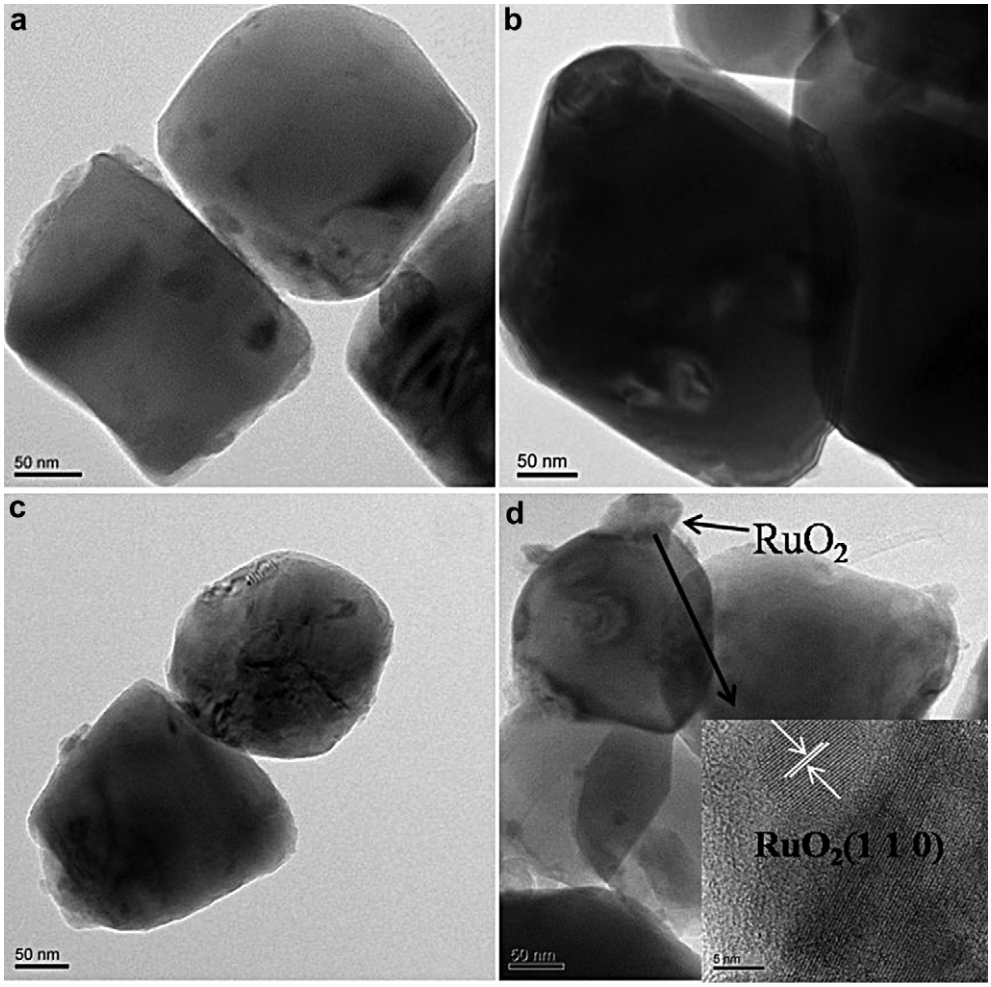

Fig. 2. TEM images and corresponding SEAD patterns (insets) of the four samples calcined at 850 °C: (a) $Li_4Ti_5O_{12}$ (b) Li:Ru = 4:0.05 (c) Li:Ru = 4:0.10 (d) Li:Ru = 4:0.15.

discharge measurements were performed in a potential range of 0.01–2.5 V *vs.* Li under different current densities.

3. Results and discussion

The precursors of with difference Ru contents were calcined at 850 °C. Fig. 1 shows the XRD patterns of those sintered powders. As reference, the standard diffraction peaks of $Li_4Ti_5O_{12}$ with JCPDS file number 49-0207 and RuO_2 with number 65-2824 are presented. The main diffraction peaks of all investigated samples can be indexed as cubic spinel $Li_4Ti_5O_{12}$. When x is less than 0.05, no obvious impurity peaks can be found. This suggests that only one phase with a structure of $Li_4Ti_5O_{12}$ exists. This implies that the precursor of Li–Ti–Ru–O could form the solid solution in the sintering process, producing a new phase of $Li_4Ti_{5s\ -\ x}Ru_xO_{12}$. However, some of RuO_2 was found when the x exceeds 0.15. This indicates that the doping content of Ru has exceeded the solid solubility of Ru in $Li_4Ti_5O_{12}$. The element compositions of the as-prepared materials have been shown in the Supplementary materials through the EDS analysis. It should be noted that, in the reverse microemulsion, some of additional tetrabutyl titanate was rapidly hydrolyzed to $Ti(OH)_4$ and formed titanium oxides during the subsequent sintering process, which has been detected and shown as those negligible peaks in XRD pattern.

Fig. 2 shows the TEM images of the sintered materials. The particle size grows after calcining in the range of 100–200 nm. At this nanoscale, the material can exhibit batter performance at large current densities [23]. However, in the as-prepared powder with a Ru doping content of $x = 0.15$, it is clearly noticed that some small particles are left. The interplanar spacing shown in Fig. 2(d) is about 0.32 nm corresponding to (110) lattice plane of RuO_2, which is in agreement with XRD results.

Fig. 3(a) shows the initial charge and discharge curves of the Ru-doped $Li_4Ti_5O_{12}$ electrodes at the current density of 875 mA g^{-1}. The cut-off voltage is set between 0.01 V and 2.5 V. Almost all the papers on $Li_4Ti_5O_{12}$ are in the voltage range of 2.5 to 1.0 V, so the theoretical capacity of $Li_4Ti_5O_{12}$ was considered as 175 mAh g^{-1} (3 lithium ions are inserted into $Li_4Ti_5O_{12}$). However, some reports have shown that the reversible capacity of $Li_4Ti_5O_{12}$ is higher than 175 mAh g^{-1} between 2.5 and 0.01 V, reaching as high as 293 mAh g^{-1}(5 lithium ions are inserted into $Li_4Ti_5O_{12}$) [24,25]. It can be found that the $Li_4Ti_{4.95}Ru_{0.05}O_{12}$ solid solution shows the highest specific capacity. It should be mentioned that, due to the addition of MWCNTs (which has a specific capacity of about 400 mAh g^{-1}) [26,27] and the formation of solid electrolyte interphase (SEI) film [28], the specific capacities of all investigated samples are higher than the theoretical specific capacity (293 mAh g^{-1}), especially in the initial cycle.

Fig. 3(b) illustrates the cycle performance at the current density of 5250 mA g^{-1} in the first 100 cycles. Once again, the $Li_4Ti_{4.95}Ru_{0.05}O_{12}$ solid solution shows higher capacities and the best electrochemical performance. However, with increasing the

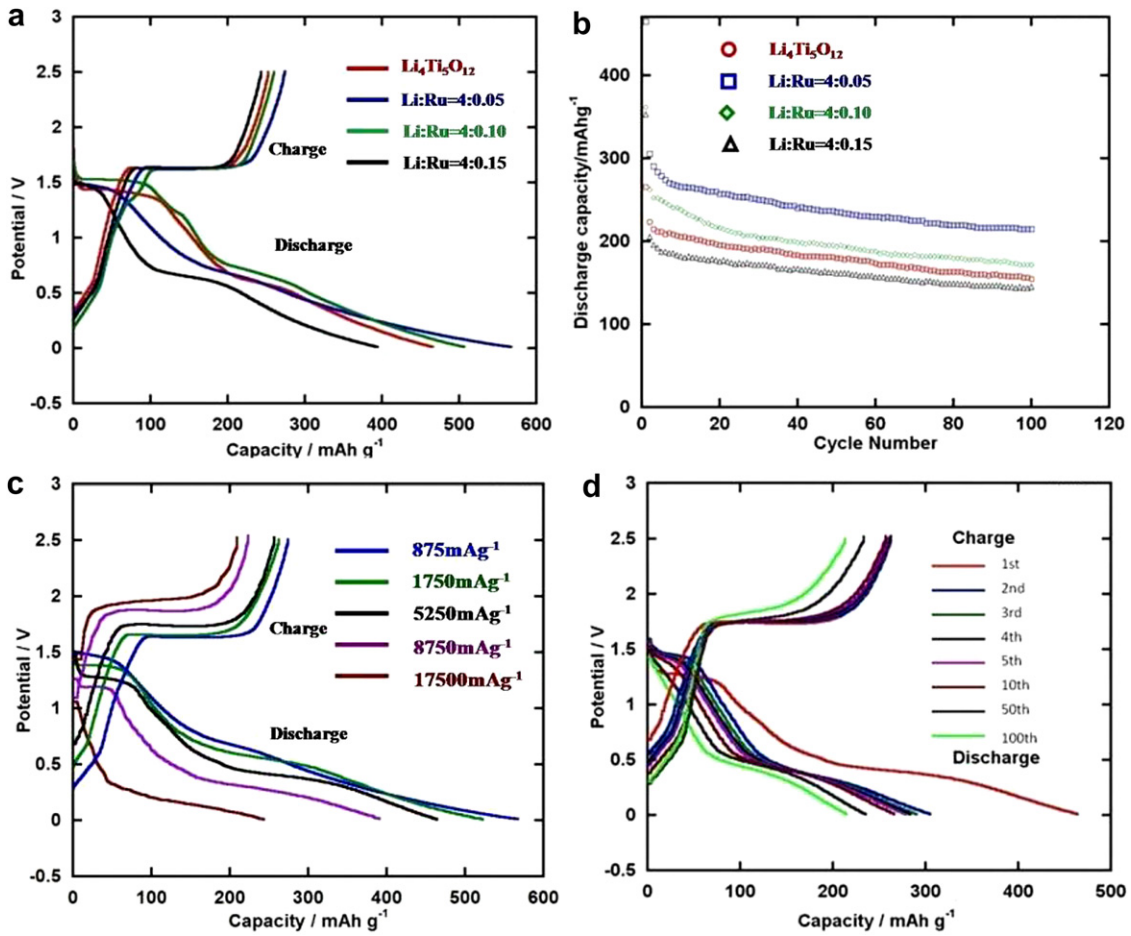

Fig. 3. Initial charge and discharge curves at 875 mA g^{-1} (a) and specific discharge capacities at 5250 mA g^{-1} (b) of different doping contents between 0.01 and 2.5 V (*vs.* Li/Li^+). (c) Initial charge and discharge curves of $Li_4Ti_{4.95}Ru_{0.05}O_{12}$ at different current densities. (d) The 1st, 2nd, 3rd, 4th, 5th, 10th, 50th and 100th charge–discharge curves of $Li_4Ti_{4.95}Ru_{0.05}O_{12}$ at 5250 mA g^{-1}.

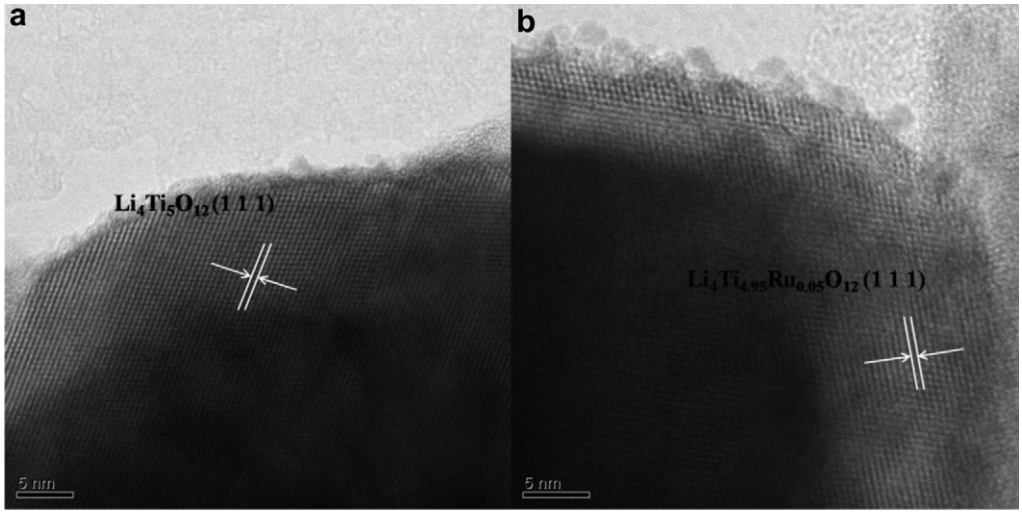

Fig. 4. HRTEM images of (a) $Li_4Ti_5O_{12}$, (b) $Li_4Ti_{4.95}Ru_{0.05}O_{12}$.

content of Ru, the specific capacity is lowering. This might be that when the doping ratio was small, $Li_4Ti_{5-x}Ru_xO_{12}$ solid solution was formed in the sintering process. With the increasing of doping amount, more RuO_2 particles attach to the surface of $Li_4Ti_5O_{12}$ particles and thereby reduce the contact area of lithium ion with $Li_4Ti_5O_{12}$ and hinder the insertion and extraction of lithium ion.

The initial charge and discharge curves of the $Li_4Ti_{4.95}Ru_{0.05}O_{12}$ at different current densities from 875 mA g^{-1} to 17500 mA g^{-1} are shown in Fig. 3(c). At the current density of 875 mA g^{-1}, the initial charge and discharge specific capacities are 274 mAh g^{-1} and 567 mAh g^{-1}, and obvious charge–discharge plateaus can be seen. Even the charge and discharge current density increases to 17500 mA g^{-1}, the corresponding capacities still remain high level, that is 209 mAh g^{-1} and 243 mAh g^{-1}. With the increase of current density the charge potential plateaus become higher while the discharge plateaus become lower and inconspicuous. This could be explained that in the charge process, the transformation is from $Li_9Ti_{4.95}Ru_{0.05}O_{12}$ to $Li_4Ti_{4.95}Ru_{0.05}O_{12}$, while in the discharge process, $Li_4Ti_{4.95}Ru_{0.05}O_{12}$ is transformed to $Li_9Ti_{4.95}Ru_{0.05}O_{12}$, and due to the repulsive interactions between neighboring lithium ions,

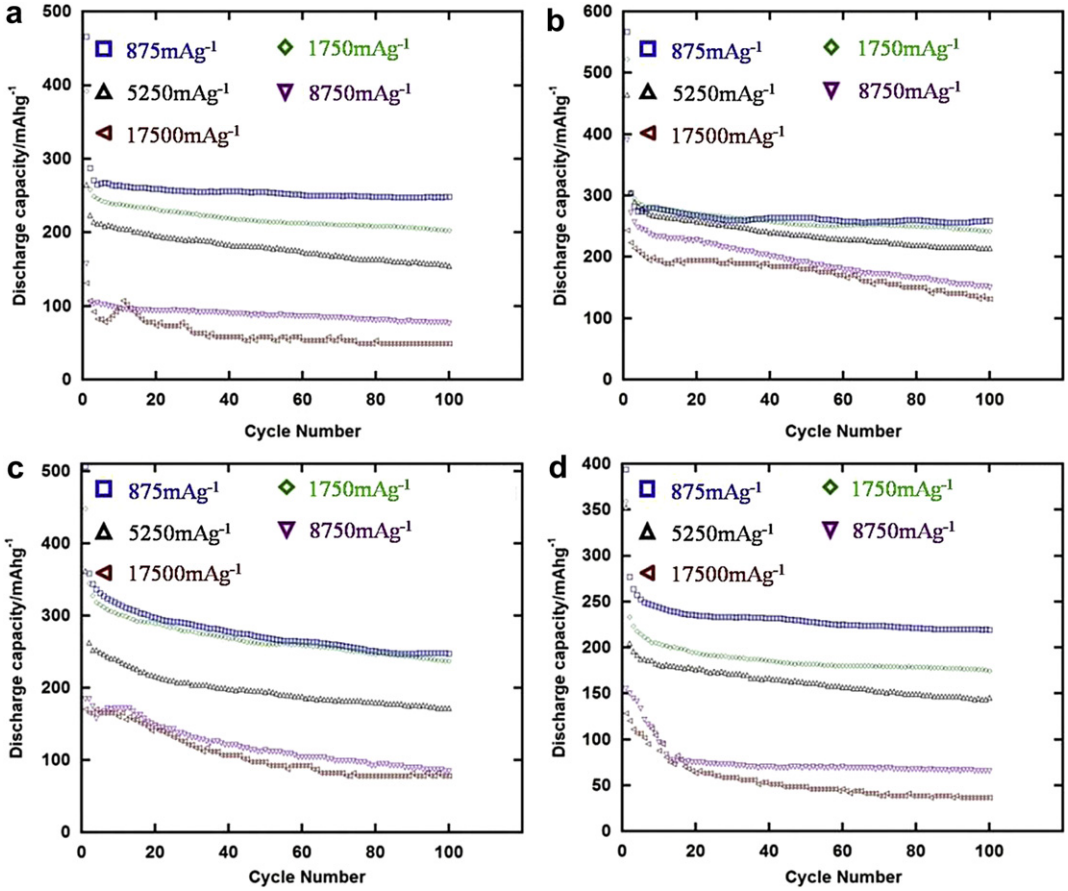

Fig. 5. Specific discharge capacity tested at different current densities over 100 cycles: (a) $Li_4Ti_5O_{12}$ (b) Li:Ru = 4:0.05 (c) Li:Ru = 4:0.10 (d) Li:Ru = 4:0.15.

the insertion of lithium is more difficult than the extraction of it [29]. As the current densities increase, the charge process can be carried out completely while the discharge process could not be carried out thoroughly and a new phase $Li_xTi_{4.95}Ru_{0.05}O_{12}$ ($4 < x < 9$) is formed. In that case, no obvious plateau of discharge curves can be found, especially at high current densities.

Fig. 3(d) shows the charge and discharge curves of $Li_4Ti_{4.95}Ru_{0.05}O_{12}$ at 5250 mA g^{-1} in the first 100 cycles. The initial specific charge and discharge capacities are 464 mAh g−1 and 257 mAh g^{-1}, respectively, which shows high specific capacity. However, the second discharge capacity declines to 305 mAh g^{-1}. The capacity loss of the following cycles is much less than that of the first two cycles, especially in the low potential. This indicates that solid electrolyte interphase (SEI) film is formed at a low potential as the reduction of electrolyte. This also can be attributed to MWCNTs (which accounts for about 60 mAh g^{-1}) where the irreversible insertion of lithium ions happens.

HRTEM images of the undoped and doped materials are shown in Fig. 4. As is shown in Fig. 4(a), the interplanar spacing is about 0.48 nm, which is corresponding to (111) lattice plane of $Li_4Ti_5O_{12}$. However, the interplanar spacing in Fig. 4(b) is about 0.50 nm corresponding to (111) lattice plane, a bit bigger than the undoped $Li_4Ti_5O_{12}$. The ionic radius of Ru^{4+} is a slight bigger than Ti^{4+}, so the doped material has a lattice expansion, which is beneficial to the insertion and extraction of lithium ions and then improves the electrochemical performance.

Fig. 5 shows the cycle performances of the four samples at different current densities. As the current density increases, the specific discharge capacity gradually decreases. As shown in Fig. 5(a), at the current density of 1750 mA g^{-1} the specific discharge capacity of $Li_4Ti_5O_{12}$ is 202 mAh g^{-1} after 100 cycles. However, when it increases to 17500 mA g^{-1}, the specific discharge capacity remains only 49 mAh g^{-1}. Fig. 5(b) shows that the specific capacity of $Li_4Ti_{4.95}Ru_{0.05}O_{12}$ is 242 mAh g^{-1} at 1750 mA g^{-1} over 100 cycles, even at 17500 mA g^{-1}, the corresponding value is 131 mAh g^{-1}, which still shows excellent performance as a battery. As the content of Ru-doping increases, the cycle performances become worse.

Fig. 6 shows the cycle performances of $Li_4Ti_{4.95}Ru_{0.05}O_{12}$ at different current densities over 500 cycles. At the current density of 1750 mA g^{-1}, the specific capacity remains 185 mAh g^{-1}. However, at a large current density of 17500 mA g^{-1}, the specific capacity still remains 73 mAh g^{-1}. The excellent performance are mainly attributed to the formation of the solid solution of $Li_4Ti_{4.95}Ru_{0.05}O_{12}$, as well as the nano-sized morphology, which can improve the conductivity, reduce ionic and electronic diffusion distance and provide a thermodynamically stable system. Most surfaces of the $Li_4Ti_{4.95}Ru_{0.05}O_{12}$ particles are wrapped with MWNT networks [30]. Because of the large aspect ratio and high electric conductivity of MWNTs, the addition of MWNTs could enhance the electrical contact among the $Li_4Ti_{4.95}Ru_{0.05}O_{12}$ particles and effectively improve the electronic conductivity and then the rate capability and cycling stability [31].

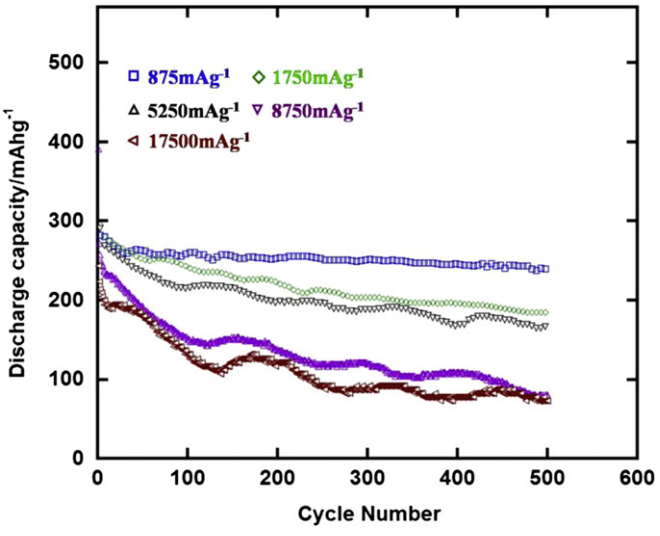

Fig. 6. Specific discharge capacity of $Li_4Ti_{4.95}Ru_{0.05}O_{12}$ tested at different current densities over 500 cycles.

4. Conclusions

In this paper, $Li_4Ti_5O_{12}$ doped with Ru was successfully synthesized in a reverse microemulsion to form a solid solution $Li_4Ti_{5-x}Ru_xO_{12}$, which shows high rate charge and discharge property. When discharged to 0.01 V, $Li_4Ti_{4.95}Ru_{0.05}O_{12}$ shows the best specific capacity and cycling stability, especially at high current densities, and this is mainly due to the formation of solid solution. Owing to the bigger ionic radius of Ru^{4+} than Ti^{4+}, the lattice constant of the doped materials is enlarged, which is in favor of the insertion and extraction of lithium ions. Even at a large current density of 17500 mA g^{-1}(about 59.7 C-rate according to the theoretic capacity of 294 mA g^{-1}), the specific discharge capacity is still 131 mAh g^{-1} over 100 cycles. All the results suggest that $Li_4Ti_{4.95}Ru_{0.05}O_{12}$ is a promising anode material for the high rate lithium ion batteries.

Acknowledgments

The work was supported by the Program for New Century Excellent Talents in University (NCET-2011-0577), Ministry of Education of China, and the Fundamental Research Funds for the Central Universities (FRF-TP-12-002B).

Appendix A. Supplementary material

Supplementary material related to this article can be found, in the online version, at http://dx.doi.org/10.1016/j.jpowsour.2012.11.092.

References

[1] B. Scrosati, J. Garche, J. Power Sources 195 (2010) 2419–2430.
[2] J.M. Tarascon, N. Recham, M. Armand, N. Chotard, P. Barpanda, W. Walker, L. Dupont, Chem. Mater. 22 (2010) 724–739.
[3] B. Scrosati, Electrochim. Acta 45 (2000) 2461–2466.
[4] J.M. Tarascon, M. Armand, Nature 414 (2001) 359–367.
[5] K. Tokumitsu, A. Mabuchi, H. Fujimoto, J. Power Sources 54 (1995) 444–447.
[6] C.Y. Ouyang, Z.Y. Zhong, M.S. Lei, Electrochem. Commun. 9 (2007) 1107–1112.
[7] S. Puunil, S.W. Kim, H.C. Shin, J. Power Sources 81–82 (1999) 248–254.
[8] E.M. Sorensen, S.J. Barry, H.K. Jung, J.R. Rondinette, J.T. Vaughey, K.R. Poeppelmeir, Chem. Mater. 18 (2006) 482–489.
[9] K. Ariyoshi, R. Yamato, T. Ohzuku, Electrochim. Acta 51 (2005) 1125–1129.
[10] S. Takai, M. Kamata, S. Fujine, K. Yoneda, K. Kanda, T. Esata, Solid State Ionics 123 (1999) 165–172.
[11] T. Ohzuku, A. Ueda, N. Yamamoto, J. Electrochem. Soc. 142 (1995) 1431–1435.
[12] P.P. Prosini, R. Mancini, L. Petrucci, V. Contini, P. Villano, Solid State Ionics 144 (2001) 185–192.
[13] S.Z. Ji, J.Y. Zhang, W.W. Wang, Y. Huang, Z.R. Feng, Z.T. Zhang, Z.L. Tang, Mater. Chem. Phys. 123 (2010) 510–515.
[14] A. Sivashanmugam, S. Gopukumar, R. Thirunakaran, C. Nithya, S. Prema, Mater. Res. Bull. 46 (2011) 492–500.
[15] T.F. Yi, J. Shu, Y.R. Zhu, X.D. Zhu, R.S. Zhu, A.N. Zhou, J. Power Sources 195 (2010) 285–288.
[16] P. Kubiak, A. Garcia, M. Womes, L. Aldon, J.O. Fourcade, P.E. Lippens, J.C. Jumas, J. Power Sources 119–121 (2003) 626–630.
[17] J. Wolfenstine, J.L. Allen, J. Power Sources 180 (2008) 582–585.
[18] B.B. Tian, H.F. Xiang, L. Zhang, Z. Li, H.H. Wang, Electrochim. Acta 55 (2010) 5453–5458.

[19] H.L. Zhao, Y. Li, Z.M. Zhu, J. Lin, Z.H. Tian, R.L. Wang, Electrochim. Acta 53 (2008) 7079–7083.
[20] H. Ge, N. Li, D. Li, C.S. Dai, D.L. Wang, Electrochem. Commun. 10 (2008) 719–722.
[21] W.J.H. Borghols, M. Wagemaker, U. Lafont, E.M. Kelder, F.M. Mulder, J. Am. Chem. Soc. 131 (2009) 17786–17792.
[22] H.F. Xiang, B.B. Tian, P.C. Lian, Z. Li, H.H. Wang, J. Alloys Compd. 509 (2011) 7205–7209.
[23] L. Kavan, J. Procházka, T.M. Spitler, M. Kalbác, M. Zukalová, T. Drezen, M. Grätzel, J. Electrochem. Soc. 150 (2003) A1000–A1007.
[24] H. Ge, N. Li, D.Y. Li, C.S. Dai, D.L. Wang, J. Phys. Chem. C 113 (2009) 6324–6326.
[25] M. Venkateswarlu, C.H. Chena, J.S. Dob, C.W. Lin, T.C. Choud, B.J. Hwang, J. Power Sources 146 (2005) 204–208.
[26] B. Gao, A. Kleinhammes, X.P. Tang, C. Bower, L. Fleming, Y. Wu, O. Zhou, Chem. Phys. Lett. 307 (1999) 153–157.
[27] C. Masarapu, V. Subramanian, H.W. Zhu, B.Q. Wei, Adv. Funct. Mater. 19 (2009) 1008–1014.
[28] P. Verma, P. Maire, P. Novák, Electrochim. Acta 55 (2010) 6332–6341.
[29] K.N. Jung, S.I. Pyun, S.W. Kim, J. Power Sources 119–121 (2003) 637–643.
[30] W. Wang, J.G. Tu, S.B. Wang, J.G. Hou, H.M. Zhu, S.Q. Jiao, Electrochim. Acta 68 (2012) 254–259.
[31] L. Kavan, R. Bacsa, M. Tunckol, P. Serp, S.M. Zakeeruddin, F.L. Formal, M. Zukalova, M. Graetzel, J. Power Sources 195 (2010) 5360–5369.